THE JOURNAL OF PHYSICAL CHEMISTRY C

Article

Cite This: J. Phys. Chem. C 2019, 123, 848−858

pubs.acs.org/JPCC

Carrier Dynamics and Interactions for Bulklike Photoexcitation of Colloidal Indium Arsenide Quantum Dots

Austin P. Spencer,[†,§] William K. Peters,[†,∥] Nathan R. Neale,[‡] and David M. Jonas*[,†]

[†]Department of Chemistry, University of Colorado, Boulder, Colorado 80309-0215, United States

[‡]Chemistry and Nanoscience Center, National Renewable Energy Laboratory, 15013 Denver West Parkway, Golden, Colorado 80401, United States

Supporting Information

ABSTRACT: The remarkable photonic and photochemical properties of colloidal quantum dots (QD) depend critically on the dynamics of carrier interactions and relaxation. Despite their importance, a quantitative experimental evaluation of these processes has proven elusive due to the inherent challenge of exactly separating single-exciton and multiexciton dynamics, whose spectroscopic signatures overlap in time, spectrum, and excitation fluence. Here, we measure pump-fluence-dependent absolute pump−probe transients of indium arsenide QDs, refreshing the sample using beam scanning to limit repetitive excitation. Focusing on the low fluence limit near the onset of biexciton formation, excitation conditions were precisely controlled and characterized by averaging Poisson-distributed excitation statistics over all three spatial dimensions of the pump and probe beam spatial profiles to determine the average excitation probability. A saturation model is developed to uniquely decompose the pump−probe signal into single-exciton and biexciton signals. This method harnesses the distinct pump-fluence scaling of absolute pump−probe signals from singly and doubly excited QDs without any assumptions regarding the relative time scales or amplitudes of single-exciton and biexciton signals. Probing in the bulklike region of the QD absorption spectrum, the signal from biexcitons is found to be 1.8 times the signal from single excitons at $T = 0$, consistent with the conventionally assumed factor of 2 within the 95% confidence intervals. The biexciton signal contains the same hot-carrier relaxation dynamics as that from single excitons, but signal from a second exciton additionally exhibits a 26 ps exponential decay attributed to Auger recombination.

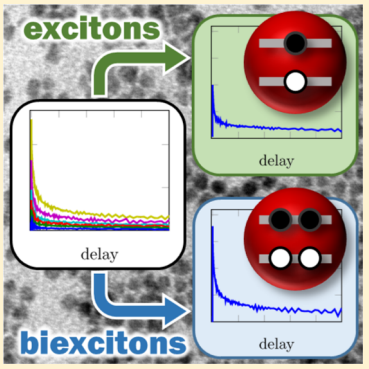

INTRODUCTION

Colloidal quantum dots (QDs) have generated significant interest in recent decades since their uniquely tunable electronic properties make QDs appealing for such applications as solar energy harvesting (in both photovoltaic and photochemical cells),[1,2] fluorescent tagging of biomolecules,[3,4] and illumination (for example, light-emitting diodes, laser diodes, and fluorescent phosphors).[5,6] Under high current or intense illumination, quantum dots have a charge carrier loss process known as Auger recombination (AR) wherein an electron and hole recombine, transferring their excess energy to a conduction-band electron or valence-band hole. AR is the inverse of impact ionization, which is one proposed mechanism for carrier multiplication (CM) or multiple-exciton generation in an isolated dot. The strong increase in impact ionization yields with excess energy[7,8] suggests that AR might also depend on excess energy, but this has not been investigated. In this context, InAs is an intriguing material because the bulk effective masses around the direct bandgap at the Γ point[9−11] indicate that excess photoexcitation energy is partitioned mainly (94%) to the electron, with the remainder left to the hole. More generally, AR is an important and ubiquitous process in QDs since it is the dominant relaxation pathway in multiply excited QDs and therefore fundamentally influences their photochemical, photovoltaic, and photonic properties.

Despite the significant link between AR and QD performance in proposed applications, many aspects of the process remain uncharacterized. One reason for this gap in understanding is that AR has proved challenging to study in a quantitative way. Of principle concern is careful control over excitation conditions to ensure an accurate accounting of the number of excitons generated per laser pulse in each QD. Unlike molecules, QDs often have highly degenerate electronic transitions with little change between ground and excited-state absorption cross-sections and so are susceptible to multiple excitation. An additional question relating to AR is whether or not pump−probe signal strength is linear with the number of excitations. Experiments typically assume that a doubly excited QD yields twice the signal of a singly excited QD, the validity of which is central to conclusions regarding the population of multiply excited QDs in studies of CM. For example, pump−probe experiments often take advantage of the large difference in time scale between AR (tens of picoseconds) and single-

Received: October 3, 2018
Revised: December 9, 2018
Published: December 10, 2018

DOI: 10.1021/acs.jpcc.8b09671
J. Phys. Chem. C 2019, 123, 848−858

exciton recombination (hundreds of picoseconds to microseconds) to quantify the fraction of QDs that initially contained multiple excitons (after pump excitation) by comparing signal amplitude before and after AR. Unfortunately, when cooling processes occur on time scales similar to or slower than AR, this method is not applicable to hot-carrier excitation, where Poisson statistics are most likely to hold.

These experimental complications motivated the thorough evaluation of carrier relaxation and interactions in InAs QDs under well-controlled conditions using degenerate pump−probe transient absorption spectroscopy presented here. Central to this goal is characterization of single- and biexciton relaxation dynamics as a function of excitation probabilities that extend into the low excitation probability regime (from 125% down to 9%) using sample exchange to minimize repetitive excitation. Excitation probability, which is the probability of excitation by the pump pulse averaged over the three-dimensional pump and probe spatial profiles, determines the proportion of QDs with 0, 1, 2, etc. excitations contributing to the pump−probe signal, and its control is important when attempting to isolate single-, bi-, and multiexciton dynamics from one another. It is also necessary to exchange the sample so that each pump−probe pulse sequence starts with an equilibrated sample.[12,13] Reported InAs QD single-exciton lifetimes are on the order of a few nanoseconds,[14−16] so the prime concern in experiments at 10 kHz laser repetition rate is the steady-state accumulation[12] of low-yield photoproducts with long lifetimes (e.g., seconds from "off states"[17−20] or QD photocharging[21]). The accumulation of "off"/photocharged QDs can be quantified by an average resampling rate.[12,13] The average resampling rate[13] ($k^{\text{resampling}}$) is the rate at which chromophores at a point in the sample are sampled by the pump during the course of the experiment. The average resampling rate is equal to the laser repetition rate (10^4 s^{-1}, here) when no sample exchange method is used (i.e., stationary sample and stationary beams) but has been reduced to 8.3 s^{-1} in this work through beam scanning.[13]

To predict the average number of excitations per QD for a given pump pulse fluence (photon flux time-integrated over a pulse) without knowledge of the frequency dependence and time dependence of the absorption cross-sections for all optically allowed excited-state absorption transitions within the laser bandwidth, assumptions must be made regarding the absorptive properties of the sample. If a chromophore's probability of absorbing a photon is unaffected by its prior history of excitation such that excitation events are independent and uncorrelated, then the number of photons absorbed by an ensemble of chromophores during a period of time will obey Poisson statistics. For this to be the case, the chromophore's absorption cross-section must *not* be affected by excitation (i.e., the ground state and all excited states must have the same absorption cross-section within the pump pulse bandwidth plus excited-state stimulated emission must lie outside the laser bandwidth). Although this rarely holds for molecular systems, it is most likely to be approximately true for QDs at low excitation density in the bulklike portions of their spectra.[22] Assuming Poisson absorption statistics, the average number of photons absorbed per QD from a single pump pulse at each point in the sample is given by $N_{eh} = \sigma_a\Phi$ where σ_a is the absorption cross-section of the QD and Φ is the pulse photon fluence (photons per unit area) at that point. To reflect the experimental conditions, the frequency dependence of σ_a and the frequency and spatial dependence of Φ must be included and averaged over. The spatial average depends on the spatial profile of both pump and probe, resulting in the spatially averaged excitation probability $\langle N_{eh}\rangle$.

A handful of studies on carrier dynamics in colloidal InAs QDs have been reported. Pijpers et al.[23] investigated multiexciton dynamics in InAs/CdSe/ZnSe core/shell/shell QDs (4.4 nm diameter core) by transient absorption spectroscopy. When pumping slightly to the blue of the "1P" transition and probing the "1S" transition, a subpicosecond carrier cooling time and a 30 ps biexciton decay time were reported. ("1S" and "1P" correspond to the transitions labeled $1S_e1S_h$ and $1P_e1P_h$, respectively, in the context of the present study.) Schaller et al.[15] performed transient absorption spectroscopy on InAs "core only" (4.3 nm diameter) and InAs/CdSe core/shell (3.9 nm diameter cores) QDs, pumping on the red side of the second exciton peak ("1P") and probing the "1S" transition. They reported a carrier cooling time of 0.66 ps (~0.5 eV/ps) for InAs/CdSe QDs, a biexciton lifetime of 8.3 ps for InAs "core only" QDs, and a single-exciton lifetime of 192 ps for InAs "core only" QDs. On the basis of transient absorption measurements, pumping at 1.55 eV and probing the first exciton peak, Ben-Lulu et al.[16] report 53 and 28 ps biexciton lifetimes and 3 and 5.2 ns single-exciton lifetimes for InAs/CdSe/ZnSe core/shell/shell QDs with first exciton peaks at 0.95 eV (5.9 nm diameter cores) and 1.1 eV (4.9 nm diameter cores), respectively. Finally, Pijpers et al.[24] report an electron relaxation time of ~0.8 ps based on the rise of the transient absorption signal when pumping the "1P" transition and probing the "1S" transition of 4.4 nm diameter InAs QDs with a bandgap of 1.1 eV. From the instrument-response limited rise time of the "1P"-pump−THz-probe signal, Pijpers et al. give an upper bound of 150 fs (or 1−2 eV/ps) for the hole cooling time. For the same THz measurements, biexciton time constants of 9.5 and 24 ps were reported in 4.0 nm diameter InAs QDs and 4.9 nm diameter InAs/CdSe/ZnSe core/shell/shell QDs, respectively. As a whole, these studies suggest a ~0.8 ps time constant for $1P_e \rightarrow 1S_e$ electron cooling and a 10−30 ps time constant for Auger recombination in ligand-passivated InAs QDs with a bandgap of approximately 1 eV. In this work, we resolve the pump-fluence dependence and temporal dynamics of hot carriers in the absolute pump−probe signal of InAs QDs by degenerately pumping and probing in the bulklike spectral region above the $1P_e1P_h$ transition. We develop a saturation model to separate single-exciton and biexciton signals based on their unique pump-fluence scaling, for the first time determining the relative amplitudes of single- and biexciton signals without assumptions regarding their relative time scales.

EXPERIMENT

Sample Preparation and Characterization. The synthesis of colloidal InAs QDs capped with trioctylphosphine (TOP) and/or trioctylphosphine oxide (TOPO) ligands is described in the Supporting Information. This synthesis is based on refs 25, 26, and 14 but differs from those procedures in that slightly higher initial precursor concentration, and smaller amounts of subsequent precursor injections were used to afford the larger particles prepared here. Also, similar to ref 14, this procedure uses both TOP and TOPO ligands for surface passivation, whereas other prior works exclusively use TOP in the InAs core synthesis. As has been shown recently by Mattoussi and co-workers for CdSe-ZnS core−shell QDs, TOP

DOI: 10.1021/acs.jpcc.8b09671
J. Phys. Chem. C 2019, 123, 848−858

weakly binds to and passivates surface heteroatoms and TOPO weakly binds to and passivates surface metal atoms.[27] Thus, the addition of TOPO to the conventional TOP solvent in InAs QD synthesis may help to passivate In and As surface sites. Anhydrous and oxygen-free conditions (see SI) were used to minimize surface oxidation. No additional surface passivation (e.g., CdSe shell) steps were taken. Characterization by transmission electron microscopy yielded a diameter distribution of 6.2 ± 0.7 nm (see SI).

The linear absorption spectrum is shown in Figure 1 along with the laser pulse spectrum. The mean QD diameter is 6.2 nm based on comparison of the central wavelength of the first exciton peak to an empirical sizing curve.[14] The measured absorbance was converted to absorption cross-section (σ_a) using the empirical scaling of absorption cross-section at the first exciton peak with QD radius reported by Yu et al.[14] The two lowest energy excitonic transitions are $1S_e1S_h$ at λ = 1199 nm and $1P_e1P_h$ at $\lambda \approx$ 900 nm. The laser pulse spectrum, centered at λ = 793 nm and with a full width at half-maximum (FWHM) bandwidth of $\Delta\lambda$ = 21 nm, overlaps with the far-blue wing of the $1P_e1P_h$ transition. The photon energy used for experiments is below the threshold for CM.

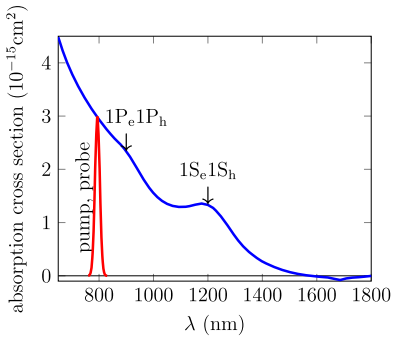

Figure 1. Visible−near-infrared absorption spectrum of colloidal InAs quantum dots (blue). The first ($1S_e1S_h$) and second ($1P_e1P_h$) exciton peaks are centered at λ = 1199 nm and $\lambda \approx$ 900 nm, respectively. The laser spectrum (red; arbitrarily scaled) is centered at $\lambda_{pu,pr}$ = 793 nm and has a full width at half-maximum bandwidth of $\Delta\lambda$ = 21 nm. The small region of negative absorbance near λ = 1700 nm is the result of imperfect background subtraction of solvent (toluene) absorption features.

Pump−Probe Spectroscopy. The output of a Ti:Sapphire regenerative amplifier (Coherent RegA; λ = 793 nm, 10 kHz repetition rate, 85 fs pulse duration) is split into pump and probe beams. An optical chopper (3501, New Focus) that is synchronized (i.e., phase-locked) to the 4th subharmonic of the laser repetition rate amplitude modulates the pump beam at 2.5 kHz (two pulses transmitted and two pulses blocked in each cycle) and is phased such that pulse clipping is minimized. Pump and probe beams then enter an interferometer that controls the time delay (T) of the probe pulses relative to the pump pulses. From the interferometer, parallel (but noncollinear) beams propagate into a beam scanning apparatus[13] that enables an average resampling rate of 8.3 s^{-1} for the measurements reported here. The all-reflective optics beam scanning apparatus uses a fast steering mirror (FSM) to move the pump−probe focal spot in a repeating spiral pattern with respect to the stationary sample such that the laser photon flux (and consequently the time-averaged excitation) is spread over a ∼6.3 mm^2 area of the sample cell, reducing repetitive excitation. Pump and probe beams are focused to a common point with a beam focal spot intensity FWHM ($d_{1/2}$) of 48 μm (see SI).

The electrical signal from the probe photodiode is filtered and amplified by a gated integrator (SR250, Stanford Research Systems), which time-integrates the single pulse waveform from the photodiode during a short time window (on the order of the response time of the detector) and amplifies the voltage. The output is then routed to a lock-in amplifier (SR830, Stanford Research Systems) that is referenced to the optical chopper. The lock-in amplifier isolates and amplifies components of its input waveform that oscillate at the same frequency as, and in phase with, the optical chopper. The resulting pump−probe signal is read digitally from the lock-in amplifier by a PC executing a LabVIEW program that controls

Table 1. Experimental Incident Pump Pulse Energy U_0, Maximum Excitation Probability $N_{eh}(0, 0)$, and Probe-Weighted Spatially Averaged Excitation Probability $\langle N_{eh}\rangle_{r,z}$ (Equation 6)[a]

U_0 (nJ)	$N_{eh}(0, 0)$	$\langle N_{eh}\rangle_{r,z}$	$\langle P_0\rangle_{r,z}$	$\langle P_1\rangle_{r,z}$	$\langle P_2\rangle_{r,z}$	$\langle P_3\rangle_{r,z}$
0.45	0.20	0.090	0.92	0.080	4.8×10^{-3}	2.1×10^{-4}
1.00	0.45	0.20	0.82	0.15	0.020	2.0×10^{-3}
1.50	0.67	0.30	0.75	0.20	0.039	5.7×10^{-3}
1.99	0.89	0.40	0.69	0.24	0.059	0.012
3.74	1.67	0.75	0.52	0.29	0.13	0.044
6.23	2.79	1.25	0.37	0.28	0.18	0.097

U_0 (nJ)	$\frac{\langle P_1\rangle_{r,z}}{1-\langle P_0\rangle_{r,z}}$ (%)	$\frac{\langle P_2\rangle_{r,z}}{1-\langle P_0\rangle_{r,z}}$ (%)	$\frac{\langle P_3\rangle_{r,z}}{1-\langle P_0\rangle_{r,z}}$ (%)	$\frac{\langle P_1\rangle_{r,z}}{\sum_n n\langle P_n\rangle_{r,z}}$ (%)	$\frac{2\langle P_2\rangle_{r,z}}{\sum_n n\langle P_n\rangle_{r,z}}$ (%)	$\frac{3\langle P_3\rangle_{r,z}}{\sum_n n\langle P_n\rangle_{r,z}}$ (%)
0.45	94	5.6	0.25	89	11	0.7
1.00	87	11	1.1	77	20	3.0
1.50	82	16	2.3	68	26	5.7
1.99	77	19	3.7	60	30	8.6
3.74	61	26	9.1	39	34	18
6.23	45	29	15	23	29	23

[a] $\langle P_n\rangle_{r,z}$ (eq 5) is the spatially averaged probability of exciting a QD n times based on Poisson absorption statistics at each point in the sample. $\langle P_n\rangle_{r,z}/(1 - \langle P_0\rangle_{r,z})$ is the fraction of excited QDs that have n excitons and $n\langle P_n\rangle_{r,z}/\sum_m m\langle P_m\rangle_{r,z}$ is the fraction of signal arising from QDs with n total excitons on the assumption that the signal is linearly proportional to the number of excitons. Absorption cross-section, σ_a (λ = 793 nm) = 2.979×10^{-15} cm^2; beam spot size, w = 41 μm; optical density, OD(λ = 793 nm) = 0.10.

DOI: 10.1021/acs.jpcc.8b09671
J. Phys. Chem. C 2019, 123, 848−858

data collection. The signal is averaged 3−10 times at each time delay in a scan, and 3−25 scans are collected and averaged.

The beam scanning apparatus used to minimize repetitive excitation artifacts is fully described in ref 13. A discussion of how to minimize such artifacts in various photophysical regimes is given in ref 12. Because the excited-state lifetime is 5 orders of magnitude shorter than the laser repetition period, a 23% shot-to-shot pulse overlap is acceptable and the pattern is designed to minimize the resampling rate to prevent steady-state accumulation of low-yield long-lived photoproducts often attributed to photocharging. The signal from shot-to-shot overlap between the probe pulse and the pump pulse from the previous laser shot is neutralized by phased lock-in detection at $k_{laser}/4$.[13] As in ref 13, the scan pattern fills a circular annulus with ∼3 mm outside diameter and ∼1 mm inside diameter over a 0.5 s period, yielding an average resampling rate of 8.3 s^{-1}. Saturation experiments at 1 ns pump−probe delay were performed with two different resampling rates to determine whether this resampling rate was sufficiently low for the InAs QDs studied here (see SI). These measurements put an upper bound of 2 ms on the quantum yield−lifetime product ($\phi_{LLS} \times \tau_{LLS}$) for photocharging of this InAs QD sample; with a 8.3 s^{-1} resampling rate, eq S1 of the SI predicts that accumulated steady-state photocharging would be effectively suppressed to below a few percent even at an excitation probability of 200%.

Pump−probe transients from $T = -1$ ps to 1 ns were collected with a 1 nJ probe pulse energy (E_{pr}) and at pump pulse energies (E_{pu}) ranging from 0.45 to 6.23 nJ (see Table 1). The pump−probe signal was confirmed to be linear with respect to sample optical density (to within 10% relative to the signal maximum) at both short ($T = 0$) and long ($T = 1$ ns) time delays for optical densities of 0.016 and 0.10, although at an optical density of 0.37 this was no longer the case. Scaling of pump−probe signal with probe pulse energy was also tested. At a probe pulse energy of 1 nJ, the signal was found to be 99 ± 15% of the linear extrapolation from low pulse energy.[28]

The probe-weighted spatially averaged excitation probability induced by the pump pulse was calculated for each experimental pump pulse energy. For simplicity, pump and probe beams were approximated such that they (a) overlap perfectly through the entire sample cell, (b) have identical circular Gaussian intensity profiles, (c) have identical spectra, (d) are well collimated over the length of the sample cell (Rayleigh range $z_R = 6.7$ mm), (e) are attenuated exponentially as a function of depth into the sample (i.e., pump and probe pulse absorptions each individually obey the Beer−Lambert law so that their pulse propagation can be described with linear optics even though the small effect of the pump on probe transmission is a nonlinear optical effect), and (f) have a frequency bandwidth that is small compared to both their central frequency and the bandwidth of overlapping features in the sample absorption spectrum such that the pulse bandwidth can be neglected (variation in optical density within the pulse FWHM bandwidth is less than 5%). Under these approximations, the photon fluences of pump and probe beams are described by Gaussian beam spatial profiles (chapter 17.1, eq 6 of Siegman),[29] given by

$$h(r, z) = \frac{2}{\pi w^2} \exp\left(-\frac{2r^2}{w^2}\right) \exp(-\alpha z) \tag{1}$$

where r is the radial polar coordinate perpendicular to the axis along which the beam propagates (z), w is the beam waist or focused spot size [$h(r = w, z = 0)/h(r = 0, z = 0) = 1/e^2$], $\alpha = [\mathrm{OD} \ln(10)]/L$ is the intensity attenuation coefficient at the center of the pulse spectrum, OD is the sample optical density, and L is the sample path length. The beam spot size is related to the FWHM diameter ($d_{1/2}$) of beam intensity through $w = d_{1/2}/\sqrt{2 \ln 2}$ so that $d_{1/2} = 48$ μm corresponds to $w = 41$ μm. (Note that there is a change in notation from ref 13; $d_{1/2}$ here is equal to w_0^{FWHM} of ref 13. This change was made to use waist w consistently with ref 29 here.) The beam spatial profile at the sample cell entrance ($z = 0$) has unit area: $\int_0^\infty h(r, z = 0) 2\pi r \, dr = 1$ where the factor of 2π arises from integration over the angle θ, on which the beam spatial profile does not depend. Multiplying eq 1 by the number of incident pump pulse photons [$N_{pu}^0 = U_0/(\hbar\omega)$ where U_0 is the incident pump pulse energy] yields the pump pulse photon fluence

$$\Phi_{pu}(r, z) = N_{pu}^0 \, h_{pu}(r, z) = \frac{U_0}{\hbar\omega} h_{pu}(r, z) \tag{2}$$

where variables with a subscript "pu" relate to the pump pulse. Subsequent multiplication of the pump pulse photon fluence in eq 2 by the absorption cross-section (σ_a) of the QD sample at the central frequency of the pump pulse gives the excitation probability as a function of position within the sample

$$N_{eh}(r, z) = \Phi_{pu}(r, z)\sigma_a \tag{3}$$

The number of absorbed photons per QD is assumed to obey Poisson statistics although this cannot be rigorously true since it predicts that in the absence of fast relaxation during the pulse, there would be no pump−probe signal during pulse overlap, in contradiction to experimental observation. On the other hand, there is no measurable deviation (less than 1%) from the linear relationship between pump absorption and pump pulse energy (see SI) predicted by Poisson statistics, although Poisson statistics is not required for such linear absorption versus pulse energy. (For example, a harmonic oscillator has no nonlinear response and the same net linear absorption for all pulse energies but has different level population statistics. Noninteracting carriers have the evenly spaced energy levels of a harmonic oscillator.) The probability of a QD having n excitations

$$P_n(r, z) = \frac{[N_{eh}(r, z)]^n \exp[-N_{eh}(r, z)]}{n!} \tag{4}$$

is then calculated using the Poisson distribution with N_{eh} as the mean. The Poisson probability coefficients for $n = 0, 1, 2, \ldots$ in eq 4 are spatially averaged over the probe beam spatial profile

$$\langle P_n \rangle_{r,z} = \frac{\int_0^\infty 2\pi r \, dr \int_0^L dz \, P_n(r, z) h_{pr}(r, z)}{\int_0^\infty 2\pi r \, dr \int_0^L dz \, h_{pr}(r, z)} \tag{5}$$

by numerical integration. The subscript "pr" on the right-hand side in eq 5 indicates that the spatial average is weighted by the *probe* spatial profile. Equations 1 and 5 show that in experiments with $w_{pr} \ll w_{pu}$ and $\alpha L \ll 1$, $\langle P_n \rangle_{r,z}$ approaches $P_n(0, 0)$ over spatial regions with appreciable probe fluence. This approach has been used[30] for static and flowing quantum dot samples. Note that even if the underlying probability of excitation at each point in the sample has a Poisson distribution, the probe-weighted spatially averaged Poisson coefficients $\langle P_n \rangle_{r,z}$ do not obey a Poisson distribution, although they approach the underlying distribution as U_0 goes to zero.

DOI: 10.1021/acs.jpcc.8b09671
J. Phys. Chem. C 2019, 123, 848−858

Finally, the probe-weighted spatially averaged excitation probability

$$\langle N_{eh}\rangle_{r,z} = \sum_{n=1}^{\infty} n\,\langle P_n\rangle_{r,z} \tag{6}$$

is calculated. The probe-weighted spatially averaged excitation probability is linearly proportional to the pump pulse energy: $\langle N_{eh}\rangle_{r,z} = (0.201\ \mathrm{nJ}^{-1})U_0$ for the conditions of these experiments, in which bulklike excitation prevents band-filling.

Table 1 summarizes the excitation conditions predicted by the above-described spatially averaged Poisson excitation probability model for the pump pulse energies used in this work. $\langle N_{eh}\rangle_{r,z}$ ranges from 0.09 to 1.25 and follows a linear relationship relative to the excitation probability in the center of the pump beam at the sample entrance, $N_{eh}(0, 0)$. The fraction of pump-excited QDs with two excitations (i.e., initially excited biexcitons), given by $\langle P_2\rangle_{r,z}/(1 - \langle P_0\rangle_{r,z})$, is significantly less than the fraction of singly excited QDs for all pump pulse energies and much less for most, indicating that these experiments probe the low-photon-flux threshold region for biexciton generation through double excitation. $n\langle P_n\rangle_{r,z}/\sum_m m\langle P_m\rangle_{r,z}$ gives the fraction of the pump–probe signal arising from QDs with n initial excitations under the assumption that signal scales linearly with the number of excitons. Although single excitons dominate the overall pump–probe signal at the lowest pulse energies, multiexcitons generate the majority of the signal at the two highest pulse energies.

RESULTS AND DISCUSSION

Absolute Pump–Probe Transients. Absolute pump–probe transients over the full 1 ns range of time delays are shown in Figure 2. The absolute pump–probe signal is the change in the number of transmitted probe photons (ΔN) caused by prior pump excitation (compared to without pump excitation) divided by the total number of incident probe photons ($N_0 = 4.0 \times 10^9$ photons). No ad hoc scaling or "tail matching" is employed. Pump–probe transients at a range of excitation probabilities were collected in the following order: $\langle N_{eh}\rangle_{r,z}$ = 75, 125, 30, 20, 9.0, and 40%. To correct for small accumulated errors in delay stage position due to occasional mis-steps (a second harmonic autocorrelation recorded immediately after the experiment showed time zero changes by +20 fs compared to the time zero immediately before the experiment), the pump–probe delay axes were adjusted such that the rise of the signal coincides between transients. This involved a +10 fs shift for transients with $\langle N_{eh}\rangle_{r,z}$ = 40% and $\langle N_{eh}\rangle_{r,z}$ = 125% as well as a +20 fs shift for the $\langle N_{eh}\rangle_{r,z}$ = 75% transient. An increase in signal size with increasing excitation probability is visually apparent. When normalized by excitation probability, as in the bottom panel of Figure 2, the four lowest excitation transients are in good agreement at early times. However, the 75 and 125% excitation probability transients lie slightly below the others starting at time zero (see inset in the bottom panel of Figure 2), possibly indicating saturation of the pumped transition. This trend persists through T = 1 ns.

Saturation Model. To model the power dependence of the signal, transients were fit to a two-level system saturation model. This model relates pump pulse energy (or, equivalently, excitation probability) to signal amplitude through

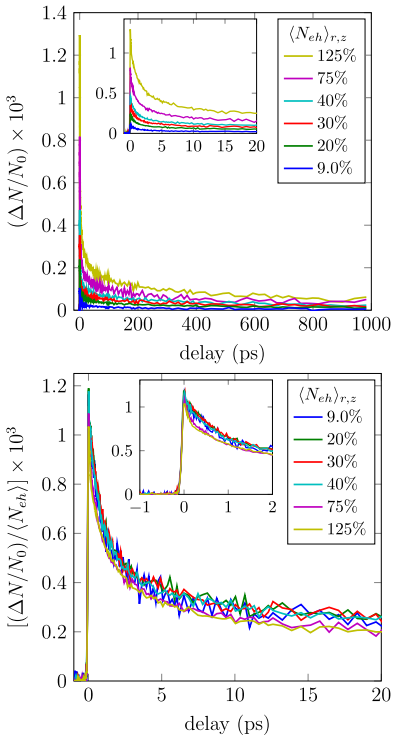

Figure 2. Pump–probe transients for probe-weighted spatially averaged excitation probabilities ranging from 9 to 125%. In the top panel, signal ($\Delta N/N_0$) is plotted as the change in number of transmitted probe photons per incident probe photon, multiplied by a factor of 10^3, with an inset highlighting the initial 20 ps. In the bottom panel, the signal is divided by the spatially averaged excitation probability ($\langle N_{eh}\rangle_{r,z}$) with an inset highlighting the initial 2 ps.

$$S_{pp}^{sat}(U_0; x, y, T) = \frac{x(T)U_0}{1 + y(T)U_0} \tag{7}$$

where $S_{pp}^{sat}(U_0; x, y, T)$ is the pump–probe signal, $x(T)$ is the slope of pump–probe signal with pump pulse energy in the low pulse energy limit, U_0 is the incident pump pulse energy, and $y(T) = 1/U_{sat}(T)$ is the inverse of the saturation pump pulse energy. When $U_0 = U_{sat}(T)$, the signal is half of its linear extrapolation from low energy given by

$$S_{pp}^{lin}(U_0; x, T) = x(T)U_0 \tag{8}$$

which we term the linear reconstruction. Equation 8 is the first-order term of the Taylor series expansion of eq 7 around U_0 = 0. The linear reconstruction is expected to contain dynamics from QDs that absorb one pump photon (single-exciton QDs) since these signal components are linear in pump excitation. Differences between the saturated signal (eq 7) and the linear reconstruction (eq 8) are indicative of signal components that are not linear with pump excitation and can arise from a number of sources, including nonlinear optical saturation of a pumped transition (for saturation at early time delays), Auger recombination (for saturation at late time delays), and repetitive excitation effects. The saturation model (eq 7) was fit to the series of transients independently at each pump–probe time delay T (see SI). Examples of saturation fits to the pump–probe signal at T = 500 fs, T = 20 ps, and T = 1 ns are shown in Figure 3.

As U_0 and $\langle N_{eh}\rangle_{r,z}$ are linearly related, saturation fits in this study were calculated as a function of $\langle N_{eh}\rangle_{r,z}$. Reported values

DOI: 10.1021/acs.jpcc.8b09671
J. Phys. Chem. C 2019, 123, 848–858

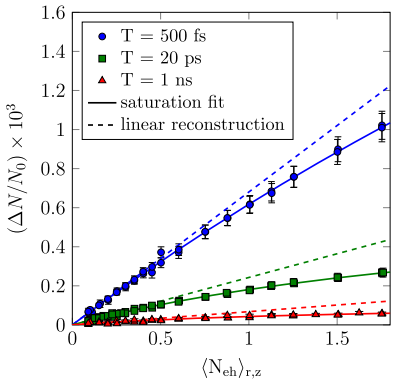

Figure 3. Pump–probe signal, $\Delta N/N_0$, measured as a function of probe-weighted spatially averaged excitation probability, $\langle N_{eh} \rangle_{r,z}$, at pump–probe delays of T = 500 fs (blue circles), T = 20 ps (green squares), and T = 1 ns (red triangles) with saturation fits (solid lines) and the corresponding linear reconstructions (dashed lines). Sample path length, L = 1 mm; optical density, OD(λ = 793 nm) = 0.1; laser repetition rate, k_{laser} = 10 kHz; beam spot size, w = 41 μm; average resampling rate, $k^{resampling}$ = 8.3 s^{-1}.

of $x(T)$ and $y(T)$ are in units of $(\Delta N/N_0)/\langle N_{eh} \rangle_{r,z}$ and $1/\langle N_{eh} \rangle_{r,z}$, respectively.

The probe-weighted spatially averaged probability of a QD being excited at least once initially by the pump pulse is given by $1 - \langle P_0 \rangle_{r,z}$. Since the Auger recombination is significantly faster than single-exciton recombination[15] through radiation or internal conversion, at pump–probe delays much longer than the Auger recombination lifetime but much shorter than the single-exciton recombination lifetime, all initially excited QDs have exactly one exciton regardless of the initial number of excitations. In this regime of pump–probe delays, the pump pulse energy dependence of the signal is expected to go as $1 - \langle P_0 \rangle_{r,z}$ (see Supporting Information).

Even at delays for which significant single-exciton recombination may have taken place, as long as the time scale of AR is much shorter than both T and the time scale of single-exciton recombination, the pump–probe signal is expected to be proportional to $1 - \langle P_0 \rangle_{r,z}$. To test this expectation, the pump–probe signal at T = 1 ns is compared to $1 - \langle P_0 \rangle_{r,z}$ in Figure 4. In the low excitation probability limit (below the lowest excitation probability used here), $\langle N_{eh} \rangle$ becomes equal to $1 - \langle P_0 \rangle_{r,z}$, resulting in a linear relationship between $S_{pp}(T)$ and $\langle N_{eh} \rangle$. When $1 - \langle P_0 \rangle_{r,z}$ is multiplied by x(1 ns) such that the linear components of $1 - \langle P_0 \rangle_{r,z}$ and S_{pp}(1 ns) are equal (green dashed line), it is clear that x(1 ns)·$(1 - \langle P_0 \rangle_{r,z})$ falls below S_{pp}(1 ns) for $\langle N_{eh} \rangle_{r,z} > 1$. When $1 - \langle P_0 \rangle_{r,z}$ is instead scaled by a multiplicative factor a (red solid line) that minimizes the least square residual relative to S_{pp}(1 ns), we observe good qualitative agreement in pump pulse energy scaling. Although x(1 ns) < a, this deviation is not statistically significant since a falls within the 95% confidence interval of x(1 ns). This agreement corroborates the excitation statistics calculated using Poisson absorption statistics and spatial averaging.

Using the fit parameters $x(T)$ and $y(T)$ at each time delay T, the linear signal component (eq 8) can be calculated. This reconstruction agrees well at early pump–probe delays with the $\langle N_{eh} \rangle_{r,z}$ = 0.20 transient, as shown in top panel of Figure 5, and the $\langle N_{eh} \rangle_{r,z}$ = 0.090 transient. At late pump–probe delays (T > 500 ps), however, the linear component lies 6 and 12% higher than the saturation fit for $\langle N_{eh} \rangle_{r,z}$ = 0.090 and $\langle N_{eh} \rangle_{r,z}$ = 0.20, respectively. This comparison suggests that the transients with the lowest probe-weighted spatially averaged excitation probabilities are dominated by single-exciton dynamics but contain small, yet measurable, biexciton contributions that decay through AR. This conclusion agrees quantitatively with the predicted late-T signal saturation (relative to the linear component) due to AR, which is given by $(1 - P_0)/\sum nP_n$. In

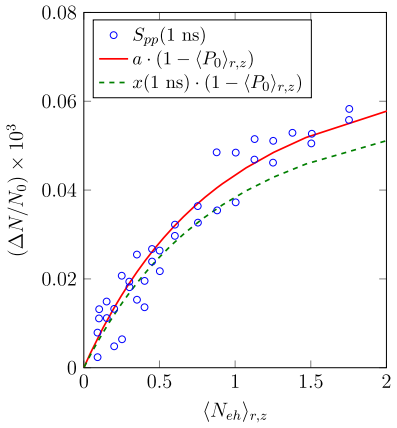

Figure 4. Pump–probe signal, $\Delta N/N_0$, measured as a function of probe-weighted spatially averaged excitation probability, $\langle N_{eh} \rangle_{r,z}$ at a pump–probe delay of T = 1 ns (blue circles) compared to the fraction of QDs initially excited by the pump pulse, $1 - \langle P_0 \rangle_{r,z}$, multiplied by the best fit parameter $a = (7.7 \pm 0.3) \times 10^{-5}$ (solid red line) or by x(1 ns) = $(6.8 \pm 1.7) \times 10^{-5}$ (dashed green line) from a saturation fit to the shown pump–probe signal data. The chosen value of a minimizes the residuals between a·$(1 - \langle P_0 \rangle_{r,z})$ and S_{pp}(1 ns) in a linear least squares sense. Sample path length, L = 1 mm; optical density, OD(λ = 793 nm) = 0.1; laser repetition rate, k_{laser} = 10 kHz; beam spot size, w = 41 μm; average resampling rate, $k^{resampling}$ = 8.3 s^{-1}.

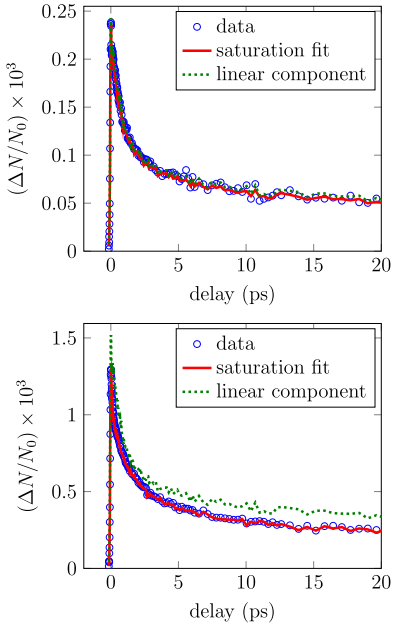

Figure 5. Pump–probe transients (blue circles) with $\langle N_{eh} \rangle_{r,z}$ = 20% (top panel) and $\langle N_{eh} \rangle_{r,z}$ = 125% (bottom panel) and their respective linear components (dashed green line) from saturation model fits (solid red line) at each time delay. Sample path length, L = 1 mm; optical density, OD(λ = 793 nm) = 0.1; laser repetition rate, k_{laser} = 10 kHz; beam spot size, w = 41 μm; average resampling rate, $k^{resampling}$ = 8.3 s^{-1}.

DOI: 10.1021/acs.jpcc.8b09671
J. Phys. Chem. C 2019, 123, 848–858

contrast, the linear component overestimates the signal size of the $\langle N_{eh}\rangle_{r,z} = 1.25$ transient by ~15% at the earliest delays, as shown in the bottom panel of Figure 5, indicating significant saturation of pump excitation at the highest pump pulse energy used. This initial saturation implies that the initial excitation number distribution is not Poisson at the highest pump pulse energy.

Reconstructed Signals for Initially Singly and Doubly Excited Particles. To separate pump−probe signals for QDs that are initially singly excited and doubly excited by the pump pulse, a procedure relying on the distinct scaling of initially excited multiexcitonic signal components with pump pulse energy was developed.[28] Saturation fits to the pump−probe transients at each pump−probe delay are taken as a complete description of the time and pump pulse energy dependence of the experimental pump−probe signal. The Taylor series expansion of the saturation model is given by

$$S_{pp}^{sat}(T) = \sum_{n=1}^{\infty} x(T)[-y(T)]^{n-1}U_0^n = x(T)U_0 - x(T)y(T)U_0^2 + \cdots \quad (9)$$

where $x(T)$ and $y(T)$ are the saturation model parameters from eq 7 and U_0 is the incident pump pulse energy.

The probe-weighted spatially averaged probability of a QD receiving one ($\langle P_1\rangle_{r,z}$) or two ($\langle P_2\rangle_{r,z}$) pump-induced excitations can be written as power series

$$\langle P_1\rangle_{r,z} = c_1U_0 - c_2U_0^2 + \cdots \quad (10)$$

and

$$\langle P_2\rangle_{r,z} = \frac{1}{2}c_2U_0^2 + \cdots \quad (11)$$

where the c_n are constants derived from a polynomial fit to numerically calculated values of $\langle P_1\rangle_{r,z}$. For the saturation model (eq 7), the value of c_2 is positive such that a QD's second excitation eliminates a single exciton in eq 10 and generates a biexciton in eq 11. Equations 10 and 11 are constructed such that by eq 6

$$\langle N_{eh}\rangle_{r,z} = \langle P_1\rangle_{r,z} + 2\langle P_2\rangle_{r,z} + \cdots = c_1U_0 \quad (12)$$

We define

$$\langle P_1\rangle_{r,z}^{linear} = c_1U_0$$
$$\langle P_2\rangle_{r,z}^{quad} = \frac{1}{2}c_2U_0^2 \quad (13)$$

such that

$$\langle P_1\rangle_{r,z} = \langle P_1\rangle_{r,z}^{linear} - 2\langle P_2\rangle_{r,z}^{quad} + \cdots$$
$$\langle P_2\rangle_{r,z} = \langle P_2\rangle_{r,z}^{quad} + \cdots \quad (14)$$

A theoretical form for the pump−probe signal is constructed from eq 14, yielding

$$S_{pp}^{theory} = b\{\langle P_1\rangle_{r,z}E(T) + \langle P_2\rangle_{r,z}B(T) + \cdots\} = b\{\langle P_1\rangle_{r,z}^{linear}E(T) + \langle P_2\rangle_{r,z}^{quad}[B(T) - 2E(T)] + \cdots\} \quad (15)$$

where $E(T)$ is the pump−probe signal from one initially singly excited QD (single exciton) and is peak normalized, $B(T)$ is the pump−probe signal from one initially doubly excited QD (biexciton), and b is a constant specific to the experimental setup and detection sensitivity. The height of $B(T)$ is not constrained, thus allowing the common assumption that the initial pump−probe signal is strictly linear with the total number of excitations and is insensitive to their distribution [i.e., $B(0) \stackrel{?}{=} 2E(0)$] to be tested.

Substituting eq 13 into eq 15 yields

$$S_{pp}^{theory} = b\left\{c_1U_0E(T) + \frac{1}{2}c_2U_0^2[B(T) - 2E(T)] + \cdots\right\} \quad (16)$$

Equating the terms in eqs 9 and 16 that are linear in U_0 and solving for $E(T)$ gives

$$E(T) = \frac{1}{b}\left[\frac{1}{c_1}x(T)\right] \quad (17)$$

Doing the same for the quadratic terms and solving for $B(T)$ gives

$$B(T) = \frac{2}{b}\left[\frac{1}{c_1}x(T) - \frac{1}{c_2}x(T)y(T)\right] \quad (18)$$

Comparing eqs 8 and 17, it is noted that $S_{pp}^{lin}(T)$ and $E(T)$ differ only by a constant multiplicative factor and therefore have the same pump−probe delay dependence.

$E(T)$ and $B(T)$ in Figure 6 are calculated according to eqs 17 and 18 using experimentally measured $x(T)$ and $y(T)$ along with coefficients c_n derived from a smooth 9th-order polynomial fit to the calculated $\langle P_1\rangle_{r,z}$ for the underlying Poisson distribution. For the 9th-order polynomial, the lowest

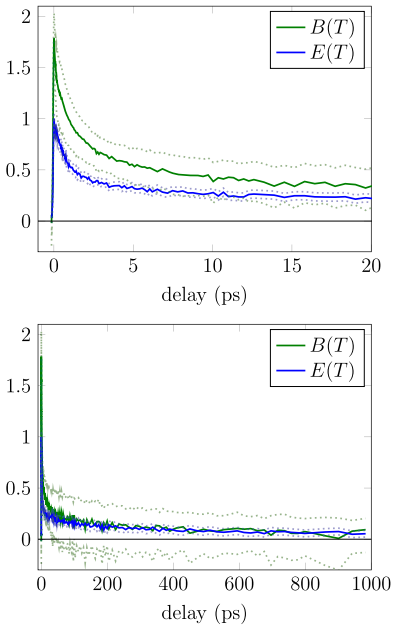

Figure 6. Reconstructed signals for initially singly excited, $E(T)$, (blue line) and doubly excited, $B(T)$, (green line) QDs with 95% confidence intervals (dotted lines). Sample path length, L = 1 mm; optical density, OD(λ = 793 nm) = 0.1; laser repetition rate, k_{laser} = 10 kHz; beam spot size, w = 41 μm; average resampling rate, $k^{resampling}$ = 8.3 s^{-1}.

DOI: 10.1021/acs.jpcc.8b09671
J. Phys. Chem. C 2019, 123, 848−858

order coefficients are numerically converged, not significantly affected by increases in polynomial order, and obey relationships expected for the polynomial coefficients of $\langle P_2 \rangle_{r,z}$, etc. Both $E(T)$ and $B(T)$ appear to contain many of the same decay time scales in similar proportions, as expected, given that initially excited biexcitons also undergo single-exciton processes such as cooling and recombination prior to, during, and after AR. At long pump−probe delays ($T > 300$ ps), $E(T)$ and $B(T)$ are equal within their uncertainties, implying that long after AR, all initially doubly excited QDs have relaxed to single-exciton states. In contrast, at short pump−probe delays ($T < 50$ ps), $B(T)$ lies above $E(T)$, a consequence of the additional signal contributed by a second exciton. Since the amplitude of $B(T)$ is not constrained, its peak height with respect to $E(T)$ is indicative of the relative signal contribution of a biexciton compared to a single exciton. This allows a test of the common assumption that a biexciton contributes exactly twice the signal of a single exciton. Figure 6 suggests that a biexciton initially yields 1.8 ± 0.4 times as much signal as a single exciton when probed in the bulklike region of the QD absorption spectrum. The time scale on which $B(T)$ converges to $E(T)$ is indicative of AR and potentially other processes requiring two excitons. Extraction of this time scale is discussed below.

Single-Exciton Dynamics. The signal for initially singly excited QDs, $E(T)$, is well described by the sum of four exponential decays and an exponentially damped cosine given by

$$S_{pp}(T) = \sum_{n=1}^{4} A_n \exp\left[-\frac{T}{\tau_n}\right] + D \cos[2\pi\nu_D T] \exp\left[-\frac{T}{\tau_D}\right] \quad (19)$$

with the parameters listed in Table 2. Multiexponential fits to the raw data in Figure 2 recover similar time constants (differing by up to 25%); since the sum of a few exponentials can effectively fit a nonexponential decay or a continuous distribution of exponential decays, the time constants may not all be individually physically significant. The decaying cosine barely survives pulse overlap (when coherent responses, such as from the solvent, may contribute) but could also have contributions from optical phonons[31−33] if phonon dephasing is distorted by hot-carrier relaxation. The four exponentials plus a damped cosine fit to $E(T)$ is illustrated in Figure 7. The fastest time constant in the fit ($\tau = 0.77$ ps) is consistent with prior reports of the $1P_e \rightarrow 1S_e$ electron cooling time. Schaller et al.[15] report a carrier cooling time of 0.66 ps in 3.9 nm diameter InAs/CdSe core/shell QDs based on the rise of "1S" signal when pumping the "1P" transition. Similarly, Pijpers et al.[24] report a 0.8 ps "1P to 1S" electron relaxation time in 4.4 nm diameter InAs QDs. The authors attribute this time scale to electron−hole coupling, proposing that electrons, as a result of their comparatively wide electronic level spacing, primarily cool through the Auger process in which a hot electron transfers energy to a hole that subsequently cools through phonon emission.[24]

Table 2. Four Exponentials Plus a Damped Cosine Fit (Equation 19) to the Signal for Initially Singly Excited QDs $E(T)$[a]

A	τ (ps)
0.50 ± 0.03	0.77 ± 0.08
0.19 ± 0.03	5.1 ± 1.2
0.12 ± 0.01	75 ± 15
0.133 ± 0.005	1061 ± 1

[a]Damped cosine parameters: $D = 0.061 \pm 0.027$, $\nu_D = 6.6 \pm 0.8$ ps^{-1}, and $\tau_D = 0.11 \pm 0.09$ ps.

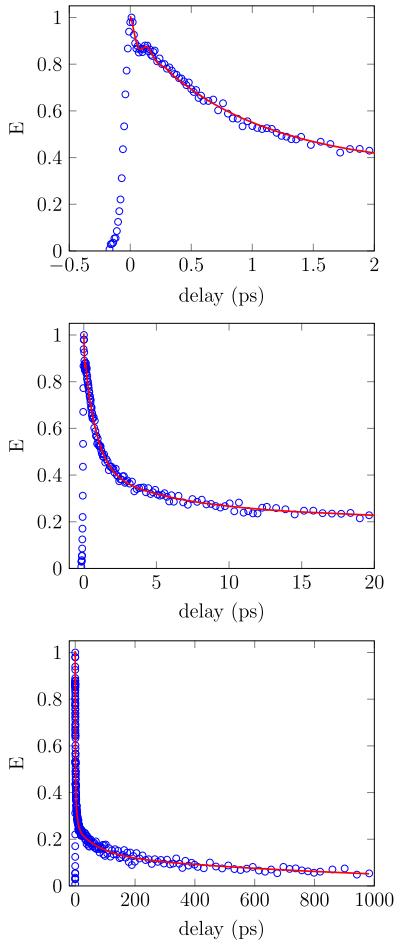

Figure 7. Reconstructed signal for initially singly excited QDs, $E(T)$, (blue circles) and a four exponential with damped cosine fit (red line). Sample path length, $L = 1$ mm; optical density, OD($\lambda = 793$ nm) = 0.1; laser repetition rate, $k_{laser} = 10$ kHz; beam spot size, $w = 41$ μm; average resampling rate, $k^{resampling} = 8.3$ s^{-1}.

The longest time constant ($\tau = 1.0$ ns) is attributed to single-exciton recombination. Reports of single-exciton lifetimes vary widely and are highly dependent on the QD surface chemistry, their exposure to oxidation, and the details of their synthesis and handling. Single-exciton lifetimes from 192 ps for 4.3 nm diameter InAs "core only" QDs[15] to 5.2 ns for 4.9 nm diameter InAs/CdSe/ZnSe core/shell/shell QDs[16] have been reported. Radiative lifetimes calculated from the Strickler−Berg relations are longer than both reported lifetimes,[14] suggesting additional nonradiative decay. If this nonradiative decay arises mainly from incomplete surface passivation, the radiative lifetime size scaling in ref 14 suggests that the TOP/TOPO ligand-capped 6.2 nm diameter InAs QDs studied here are more effectively passivated than the TOP ligand-capped 4.3 nm diameter InAs QDs studied in ref 15 but not as fully passivated as the 4.9 nm diameter InAs/CdSe/ZnSe core/shell/shell QDs in ref 16. The intermediate time constants ($\tau =$ 5.1 ps and $\tau = 75$ ps) in the single-exciton (low pump pulse

DOI: 10.1021/acs.jpcc.8b09671
J. Phys. Chem. C 2019, 123, 848−858

energy) signal are not reported in prior studies, which, unlike this work, probe the $1S_e1S_h$ transition. These time constants may indicate that probing in the bulklike region of the QD absorption spectrum is sensitive to relaxation, carrier trapping, or trap recombination processes that are not probed at the $1S_e1S_h$ transition. Carrier trapping processes can be highly heterogeneous, and even widely separated time constants might be effectively fitting an inhomogeneous distribution of quantum dots that each have a single exponential decay from trapping (see ref 34). This heterogeneous interpretation suggests partial surface passivation with QD-to-QD variation in the number or type of trap recombination sites.

Multiexciton Dynamics. In bulklike regions[22] of a QD's spectrum, it is a reasonable approximation to treat the pump−probe signal size as directly proportional to the number of electron−hole pairs (excitons) in the sample. In such a case, the signal generated by a QD in a biexciton state is twice that of a QD in a single-exciton state. A common method for quantifying the yield of biexcitons generated by the pump pulse is to compare the signal size at pump−probe delays that are short compared to AR, but long compared to carrier cooling, to the signal size at pump−probe delays that are long compared to AR, but short compared to single-exciton recombination.[35] However, this method *will not work here* due to the presence of single-exciton relaxation pathways with time constants (τ = 5.1 and 75 ps) that are on the order of the expected AR time constant (τ_{AR} = 10−30 ps). In addition, this method relies heavily on the assumption that the pump−probe signal is strictly linear with the number of excitons, which, although verified here for bulklike excitation of hot carriers, may not be justified when pumping and/or probing an excitonic transition. Instead, an alternative method is proposed.

Given the ability to separate the dynamics of initially doubly and singly excited QDs into $B(T)$ and $E(T)$, the processes unique to biexcitons can be isolated through an algebraic combination of $B(T)$ and $E(T)$. If it is assumed that

$$E(T) = X(T)$$
$$B(T) = XX(T)X(T) + X(T) \tag{20}$$

where $X(T)$ contains the signal for processes involving exactly one exciton and is peak normalized and $XX(T)$ contains the signal for processes involving exactly two excitons, then the dynamics specific to two-exciton processes can be extracted using

$$XX(T) = \frac{B(T)}{E(T)} - 1 \tag{21a}$$

Substituting eqs 18 and 17 into eq 21a yields

$$XX(T) = 2\left[1 - \frac{c_1}{c_2}y(T)\right] - 1$$
$$= 1 - 2\frac{c_1}{c_2}y(T) \tag{21b}$$

To account for the slight and experimentally insignificant difference in amplitude between $B(T)$ and $E(T)$ at late times, the ratio $B(1\text{ ns})/E(1\text{ ns})$ = 1.13 derived from the data in Figure 3 is subtracted from $B(T)/E(T)$ instead of 1.

$$XX(T) = \frac{B(T)}{E(T)} - \frac{B(1\text{ ns})}{E(1\text{ ns})} \tag{21c}$$

The result is illustrated in Figure 8 along with a single exponential fit with τ = 26 ± 5 ps. This time constant is

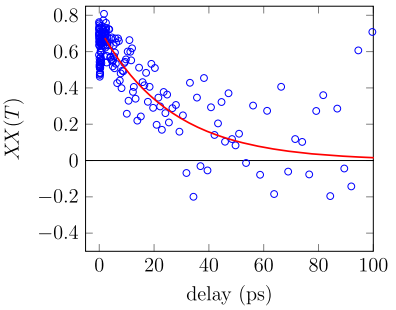

Figure 8. Ratio of signals for initially doubly and singly excited QDs, given by eq 21c (blue line) and a single exponential fit (red line). The ratio varies widely at long times where $E(T)$ and $B(T)$ tend to zero. Sample path length, L = 1 mm; optical density, OD(λ = 793 nm) = 0.1; laser repetition rate, k_{laser} = 10 kHz; beam spot size, w = 41 μm; average resampling rate, $k^{resampling}$ = 8.3 s^{-1}.

consistent with AR and is well within the 8−53 ps range of reported biexciton lifetimes for InAs QDs.[15,16,23,24] The closest comparison in terms of QD core size is a study by Ben-Lulu et al.,[16] who report a 53 ps biexciton lifetime for 5.9 nm diameter InAs/CdSe/ZnSe core/shell/shell QDs. However, their observation of a relatively long biexciton lifetime may be due to the use of core/shell structures as opposed to the as-prepared ligand-capped QDs used in the present study.

The most comparable study of similar sized as-prepared ligand-capped InAs QDs is that of Schaller et al.[15] wherein an 8.3 ps biexciton lifetime was reported for 4.3 nm diameter InAs "cores". If AR time constants scale with QD volume,[36,37] an 8.3 ps biexciton lifetime in 4.3 nm QDs would predict a 27 ps biexciton lifetime for the 6.2 nm QDs of the present study. This agrees within error with the AR lifetime reported here.

Although Schaller et al.[15] note no difference in pump−probe signal size between transients collected while the sample is "static" compared to when the sample is stirred, insufficient sample renewal can result in repetitive excitation effects such as photocharging which can complicate studies of AR.[38] Photocharged QDs can undergo trion decay, which is the nonradiative recombination of an exciton through transferring excess energy to a free charge carrier. Since trion decay occurs on time scales similar to AR, it can artificially increase the apparent biexciton yield when inadequate sample renewal leads to photocharging.[38]

CONCLUSIONS

Carrier relaxation dynamics of 6.2 nm diameter colloidal InAs QDs in the weak excitation regime have been investigated using degenerate pump−probe transient absorption spectroscopy. A beam scanning apparatus was employed to reduce repetitive excitation of the sample, reducing the resampling rate from the 10 kHz laser repetition rate to 8.3 s^{-1}. This resampling rate is low enough to prevent signal from accumulated photoproducts such as charged QDs.

Electronic relaxation following photoexcitation to the blue side of the $1P_e1P_h$ state was characterized. A saturation model was fit to transients with excitation probabilities ranging from $\langle N_{eh}\rangle$ = 9.0 to 125%, from which the linear signal was reconstructed. A comparison between the linear reconstruction

DOI: 10.1021/acs.jpcc.8b09671
J. Phys. Chem. C 2019, 123, 848−858

and a transient with $\langle N_{eh} \rangle$ = 20% demonstrates that this measurement is dominated by dynamics of singly excited QDs.

A procedure for isolating dynamics from initially singly and doubly excited QDs was developed. This method utilizes the Taylor series expansion of the saturation model along with Poisson-based calculations of the probe-weighted spatially averaged excitation probability and relies on fewer assumptions than previously reported methods.[35] Comparison of reconstructed singly excited, $E(T)$, and doubly excited, $B(T)$, QD signals near $T = 0$ indicates that a biexciton yields a factor of 1.8 ± 0.4 times the signal of a single exciton when probed in the bulklike region of the QD absorption spectrum; the conventionally assumed factor of 2 is consistent within the 95% confidence intervals for $B(T)$. This factor of ∼2 for probing in the bulklike region of the spectrum does not imply that the same factor holds for bandgap probing; quantum confined excitonic transitions may behave differently than bulklike transitions.[22] At long pump−probe delays ($T \geq 300$ ps), $B(T)$ and $E(T)$ converge to the same value within their uncertainties, lending evidence to the expectation that all initially excited biexcitons recombine through a sub-100 ps process to form single excitons at late times.

The reconstructed signal for initially singly excited QDs was well described by a four exponential plus damped cosine fit, yielding time constants of 0.77 ± 0.08 and 1061 ± 1 ps, consistent with electron cooling and single-exciton recombination, respectively, and two previously unreported time constants of 5.1 ± 1.2 and 75 ± 15 ps that may be the result of hot-carrier cooling or trapping. Alternatively, these time constants might be an effective fit to a broad inhomogeneous distribution of trapping times. The reconstructed signal for initially doubly excited QDs contains, in addition to the single-exciton dynamics, a time constant of 26 ± 5 ps (for 6.2 nm diameter QDs) that is consistent with Auger recombination. The AR lifetime reported here for 6.2 nm diameter ligand-capped QDs without an inorganic shell agrees, within error, with QD volume scaling[36,37] of the 8.3 ps literature AR lifetime for 4.3 nm diameter[15] ligand-capped InAs QDs.

■ ASSOCIATED CONTENT

Supporting Information

The Supporting Information is available free of charge on the ACS Publications website at DOI: 10.1021/acs.jpcc.8b09671.

> Materials and synthesis of InAs quantum dots, TEM images, measurement of laser beam focal spot size, tests that pump pulse absorption scales linearly with pump pulse energy, estimates of the quantum yield−lifetime product parameter for photoproducts from a repetitive excitation kinetic model, tests of the saturation model, and saturation model fits $x(T)$ and $y(T)$ (PDF)

■ AUTHOR INFORMATION

Corresponding Author

*E-mail: david.jonas@colorado.edu.

ORCID

Austin P. Spencer: 0000-0003-4043-2062
William K. Peters: 0000-0002-1270-7623
Nathan R. Neale: 0000-0001-5654-1664
David M. Jonas: 0000-0002-1085-8161

Present Addresses

[‖]Los Alamos National Laboratory, Los Alamos, New Mexico 87545, United States (W.K.P.).
[§]Department of Chemistry, Northwestern University, Evanston, Illinois 60208, United States (A.P.S.).

Notes

The authors declare no competing financial interest.

■ ACKNOWLEDGMENTS

We thank Kyle Schnitzenbaumer for help in measuring TEM images of the sample. This material is based upon work of A.P.S., W.K.P., and D.M.J. supported by the US Department of Energy, Office of Science, Office of Basic Energy Sciences, Division of Chemical Sciences, Geosciences, and Biosciences, under Award Number DE-FG02-07ER15912. This work was authored in part by Alliance for Sustainable Energy, LLC, the manager and operator of the National Renewable Energy Laboratory for the US Department of Energy (DOE) under Contract no. DE-AC36-08GO28308. Support for InAs QD synthesis was provided by the US Department of Energy, Office of Science, Office of Basic Energy Sciences, Chemical Sciences, Geosciences, and Biosciences Division.

■ REFERENCES

(1) Nozik, A. J. Quantum Dot Solar Cells. *Physica E* **2002**, *14*, 115−120.
(2) Yu, P.; Zhu, K.; Norman, A. G.; Ferrere, S.; Frank, A. J.; Nozik, A. J. Nanocrystalline TiO_2 Solar Cells Sensitized With InAs Quantum Dots. *J. Phys. Chem. B* **2006**, *110*, 25451−25454.
(3) Larson, D. R.; Zipfel, W. R.; Williams, R. M.; Clark, S. W.; Bruchez, M. P.; Wise, F. W.; Webb, W. W. Water-Soluble Quantum Dots for Multiphoton Fluorescence Imaging In Vivo. *Science* **2003**, *300*, 1434−1436.
(4) Resch-Genger, U.; Grabolle, M.; Cavaliere-Jaricot, S.; Nitschke, R.; Nann, T. Quantum Dots Versus Organic Dyes As Fluorescent Labels. *Nat. Methods* **2008**, *5*, 763−775.
(5) Shirasaki, Y.; Supran, G. J.; Bawendi, M. G.; Bulović, V. Emergence of Colloidal Quantum-Dot Light-Emitting Technologies. *Nat. Photonics* **2013**, *7*, 13−23.
(6) Jang, E.; Jun, S.; Jang, H.; Lim, J.; Kim, B.; Kim, Y. White-Light-Emitting Diodes With Quantum Dot Color Converters for Display Backlights. *Adv. Mater.* **2010**, *22*, 3076−3080.
(7) Tauc, J. Electron Impact Ionization in Semiconductors. *J. Phys. Chem. Solids* **1959**, *8*, 219−223.
(8) Dumke, W. P. Theory of Avalanche Breakdown in InSb and InAs. *Phys. Rev.* **1968**, *167*, 783−789.
(9) Madelung, O. *Physics of III-V Compounds*; Wiley Series on the Science and Technology of Materials; John Wiley & Sons, Inc.: New York, 1964.
(10) Vurgaftman, I.; Meyer, J. R.; Ram-Mohan, L. R. Band Parameters for III-V Compound Semiconductors and Their Alloys. *J. Appl. Phys.* **2001**, *89*, 5815−5875.
(11) Kim, Y.-S.; Hummer, K.; Kresse, G. Accurate Band Structures and Effective Masses for InP, InAs, and InSb Using Hybrid Functionals. *Phys. Rev. B* **2009**, *80*, No. 035203.
(12) Baranov, D.; Hill, R. J.; Ryu, J.; Park, S. D.; Huerta-Viga, A.; Carollo, A. R.; Jonas, D. M. Interferometrically Stable, Enclosed, Spinning Sample Cell for Spectroscopic Experiments on Air-Sensitive Samples. *Rev. Sci. Instrum.* **2017**, *88*, No. 014101.
(13) Spencer, A. P.; Hill, R. J.; Peters, W. K.; Baranov, D.; Cho, B.; Huerta-Viga, A.; Carollo, A. R.; Curtis, A. C.; Jonas, D. M. Sample Exchange by Beam Scanning With Applications to Noncollinear Pump−Probe Spectroscopy at Kilohertz Repetition Rates. *Rev. Sci. Instrum.* **2017**, *88*, No. 064101.
(14) Yu, P.; Beard, M. C.; Ellingson, R. J.; Ferrere, S.; Curtis, C.; Drexler, J.; Luiszer, F.; Nozik, A. J. Absorption Cross-Section and

DOI: 10.1021/acs.jpcc.8b09671
J. Phys. Chem. C 2019, 123, 848−858

Related Optical Properties of Colloidal InAs Quantum Dots. *J. Phys. Chem. B* **2005**, *109*, 7084−7087.
(15) Schaller, R. D.; Pietryga, J. M.; Klimov, V. I. Carrier Multiplication in InAs Nanocrystal Quantum Dots With an Onset Defined by the Energy Conservation Limit. *Nano Lett.* **2007**, *7*, 3469−3476.
(16) Ben-Lulu, M.; Mocatta, D.; Bonn, M.; Banin, U.; Ruhman, S. On the Absence of Detectable Carrier Multiplication in a Transient Absorption Study of InAs/CdSe/ZnSe Core/Shell1/Shell2 Quantum Dots. *Nano Lett.* **2008**, *8*, 1207−1211.
(17) Zhao, J.; Nair, G.; Fisher, B. R.; Bawendi, M. G. Challenge to the Charging Model of Semiconductor-Nanocrystal Fluorescence Intermittency From Off-State Quantum Yields and Multiexciton Blinking. *Phys. Rev. Lett.* **2010**, *104*, No. 157403.
(18) Correa, R. E.; Dauler, E. A.; Nair, G.; Pan, S. H.; Rosenberg, D.; Kerman, A. J.; Molnar, R. J.; Hu, X.; Marsili, F.; Anant, V.; et al. Single Photon Counting From Individual Nanocrystals in the Infrared. *Nano Lett.* **2012**, *12*, 2953−2958.
(19) Efros, A. L.; Nesbitt, D. J. Origin and Control of Blinking in Quantum Dots. *Nat. Nanotechnol.* **2016**, *11*, 661−671.
(20) Rabouw, F. T.; Donega, C. d. M. Excited-State Dynamics in Colloidal Semiconductor Nanocrystals. *Top. Curr. Chem.* **2016**, *374*, 58.
(21) Padilha, L. A.; Robel, I.; Lee, D. C.; Nagpal, P.; Pietryga, J. M.; Klimov, V. I. Spectral Dependence of Nanocrystal Photoionization Probability: The Role of Hot-Carrier Transfer. *ACS Nano* **2011**, *5*, 5045−5055.
(22) Cho, B.; Peters, W. K.; Hill, R. J.; Courtney, T. L.; Jonas, D. M. Bulklike Hot Carrier Dynamics in Lead Sulfide Quantum Dots. *Nano Lett.* **2010**, *10*, 2498−2505.
(23) (a) Pijpers, J. J. H.; Hendry, E.; Milder, M. T. W.; Fanciulli, R.; Savolainen, J.; Herek, J. L.; Vanmaekelbergh, D.; Ruhman, S.; Mocatta, D.; Oron, D.; et al. Carrier Multiplication and Its Reduction by Photodoping in Colloidal InAs Quantum Dots. *J. Phys. Chem. C* **2007**, *111*, 4146−4152. (b) Pijpers, J. J. H.; Hendry, E.; Milder, M. T. W.; Fanciulli, R.; Savolainen, J.; Herek, J. L.; Vanmaekelbergh, D.; Ruhman, S.; Mocatta, D.; Oron, D.; et al. Carrier Multiplication and Its Reduction by Photodoping in Colloidal InAs Quantum Dots. *J. Phys. Chem. C* **2008**, *112*, 4783−4784.
(24) Pijpers, J. J. H.; Milder, M. T. W.; Delerue, C.; Bonn, M. (Multi)exciton Dynamics and Exciton Polarizability in Colloidal InAs Quantum Dots. *J. Phys. Chem. C* **2010**, *114*, 6318−6324.
(25) Peng, X.; Wickham, J.; Alivisatos, A. P. Kinetics of II-VI and III-V Colloidal Semiconductor Nanocrystal Growth: "Focusing" of Size Distributions. *J. Am. Chem. Soc.* **1998**, *120*, 5343−5344.
(26) Cao, Y. W.; Banin, U. Growth and Properties of Semiconductor Core/Shell Nanocrystals With InAs Cores. *J. Am. Chem. Soc.* **2000**, *122*, 9692−9702.
(27) Zeng, B.; Palui, G.; Zhang, C.; Zhan, N.; Wang, W.; Ji, X.; Chen, B.; Mattoussi, H. Characterization of the Ligand Capping of Hydrophobic CdSe-ZnS Quantum Dots Using NMR Spectroscopy. *Chem. Mater.* **2018**, *30*, 225−238.
(28) Spencer, A. P. Simulation of Propagation-Distorted 2DFT Spectra of Dense Rubidium Vapor and Pump-Probe Spectroscopy of Carrier Dynamics in Colloidal Indium Arsenide Quantum Dots. PhD thesis, University of Colorado: Boulder, Colorado, 2014.
(29) Siegman, A. E. *Lasers*, 1st ed.; University Science Books: Mill Valley, CA, 1986.
(30) Midgett, A. G.; Hillhouse, H. W.; Hughes, B. K.; Nozik, A. J.; Beard, M. C. Flowing Versus Static Conditions for Measuring Multiple Exciton Generation in PbSe Quantum Dots. *J. Phys. Chem. C* **2010**, *114*, 17486−17500.
(31) Li, Y. B.; Ferguson, I. T.; Stradling, R. A.; Zallen, R. Raman Scattering by Plasmon-Phonon Modes in Highly Doped n-InAs Grown by Molecular Beam Epitaxy. *Semicond. Sci. Technol.* **1992**, *7*, 1149−1154.
(32) Cerullo, G.; De Silvestri, S.; Banin, U. Size-Dependent Dynamics of Coherent Acoustic Phonons in Nanocrystal Quantum Dots. *Phys. Rev. B* **1999**, *60*, 1928−1932.
(33) Heitz, R.; Mukhametzhanov, I.; Stier, O.; Madhukar, A.; Bimberg, D. Enhanced Polar Exciton-LO-Phonon Interaction in Quantum Dots. *Phys. Rev. Lett.* **1999**, *83*, 4654−4657.
(34) Kern, S. J.; Sahu, K.; Berg, M. A. Heterogeneity of the Electron-Trapping Kinetics in CdSe Nanoparticles. *Nano Lett.* **2011**, *11*, 3493−3498.
(35) Schaller, R. D.; Klimov, V. I. High Efficiency Carrier Multiplication in PbSe Nanocrystals: Implications for Solar Energy Conversion. *Phys. Rev. Lett.* **2004**, *92*, No. 186601.
(36) Klimov, V. I.; Mikhailovsky, A. A.; McBranch, D. W.; Leatherdale, C. A.; Bawendi, M. G. Quantization of Multiparticle Auger Rates in Semiconductor Quantum Dots. *Science* **2000**, *287*, 1011−1013.
(37) Nozik, A. J. Multiple Exciton Generation in Semiconductor Quantum Dots. *Chem. Phys. Lett.* **2008**, *457*, 3−11.
(38) McGuire, J. A.; Sykora, M.; Joo, J.; Pietryga, J. M.; Klimov, V. I. Apparent Versus True Carrier Multiplication Yields in Semiconductor Nanocrystals. *Nano Lett.* **2010**, *10*, 2049−2057.

DOI: 10.1021/acs.jpcc.8b09671
J. Phys. Chem. C 2019, 123, 848−858